Electronic Supplementary Material (ESI) for Nanoscale.

Intrinsic functional and architectonic heterogeneity of tumor-targeted protein nanoparticles

Mireia Pesarrodona [a, b, c], Eva Crosas [d], Rafael Cubarsi [e], Alejandro Sánchez-Chardi [f], Paolo Saccardo [a, , c], Ugutz Unzueta [c, g], Fabian Rueda [a, b, c], Laura Sanchez-García [a, b, c], Naroa Serna [a, b, c], Ramón Mangues [c, g], Neus Ferrer-Miralles [a, b, c], Esther Vázquez [a, b, c*], Antonio Villaverde [a, b, c*]

[a.] *Institut de Biotecnologia i de Biomedicina, Universitat Autònoma de Barcelona, 08193 Cerdanyola del Vallès, Spain.*

[b.] *Departament de Genètica i de Microbiologia, Universitat Autònoma de Barcelona, 08193 Cerdanyola del Vallès, Spain.*

[c.] *CIBER de Bioingeniería, Biomateriales y Nanomedicina (CIBER-BBN), Spain.*

[d.] *ALBA Synchrotron, Carrer de la llum, 2-26, 08290 Cerdanyola del Vallès, Spain.*

[e.] *Department of Mathematics, Campus Diagonal Sud, Edifici U, Universitat Politècnica de Catalunya, Carrer de Pau Gargallo, 5, 08028 Barcelona, Spain.*

[f.] *Servei de Microscòpia, Universitat Autònoma de Barcelona, 08193 Cerdanyola del Vallès, Spain.*

[g.] *Biomedical Research Institute Sant Pau (IIB-Sant Pau) and Josep Carreras Leukemia Research Institute, Hospital de la Santa Creu i Sant Pau, 08025 Barcelona, Spain.*

* Corresponding authors.

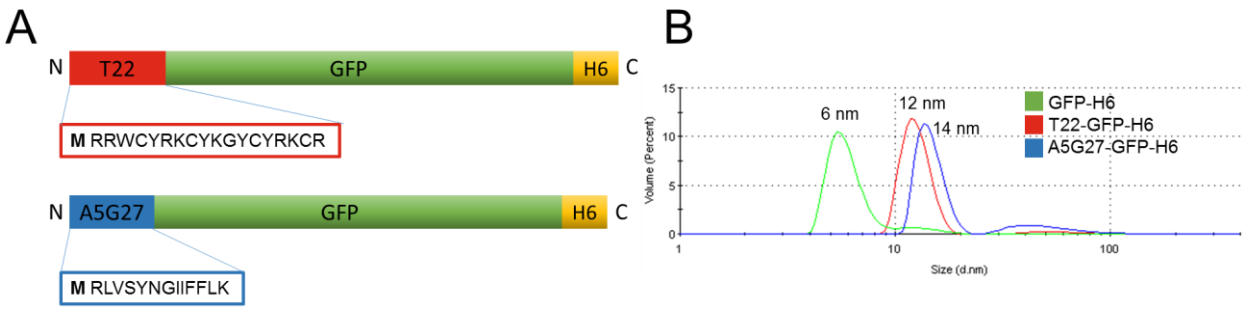

Supplementary Figure 1. Basic features of T22-GFP-H6 and A5G27-GFP-H6 building blocks. A. Modular design of T22-GFP-H6 and A5G27-GFP-H6, from amino (N) to carboxyl (C) termini. In boxes, the amino acid sequences of the cell receptor ligands that act simultaneously as architectonic tags. Further details of the amino acid sequences can be found elsewhere. The relative sizes of the protein cassettes are not accurate. B. Average size of pooled protein nanoparticles resulting from the spontaneous self-assembling of T22-GFP-H6 and A5G27-GFP-H6 building blocks and of unassembled protein control GFP-H6, determined by DLS.

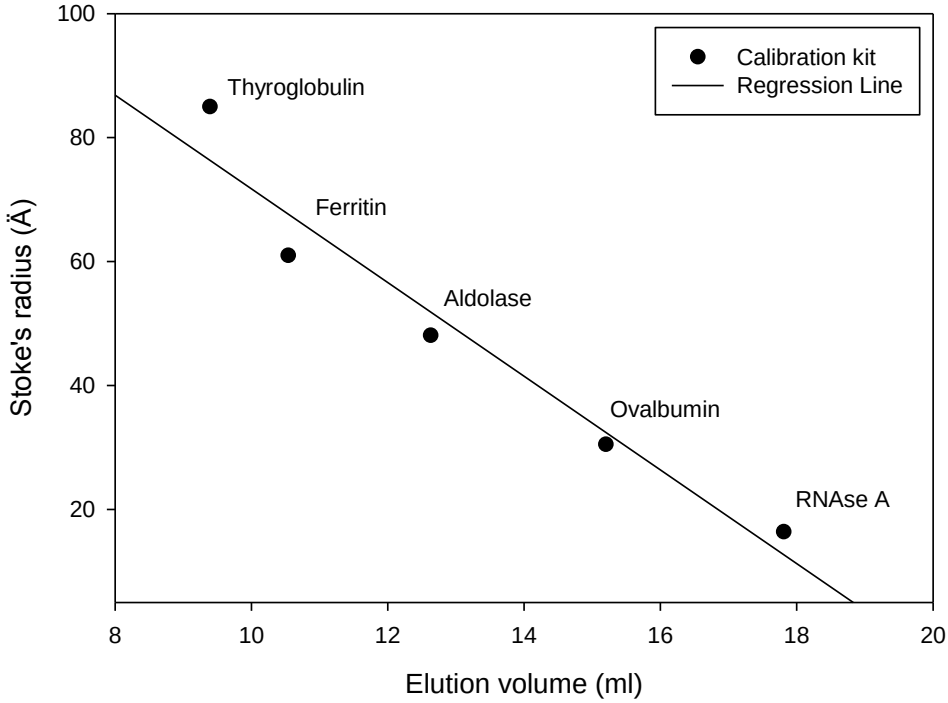

Supplementary Figure 2. SEC calibration curve using a standard calibration kit of known Stroke's radius. A regression line is shown.

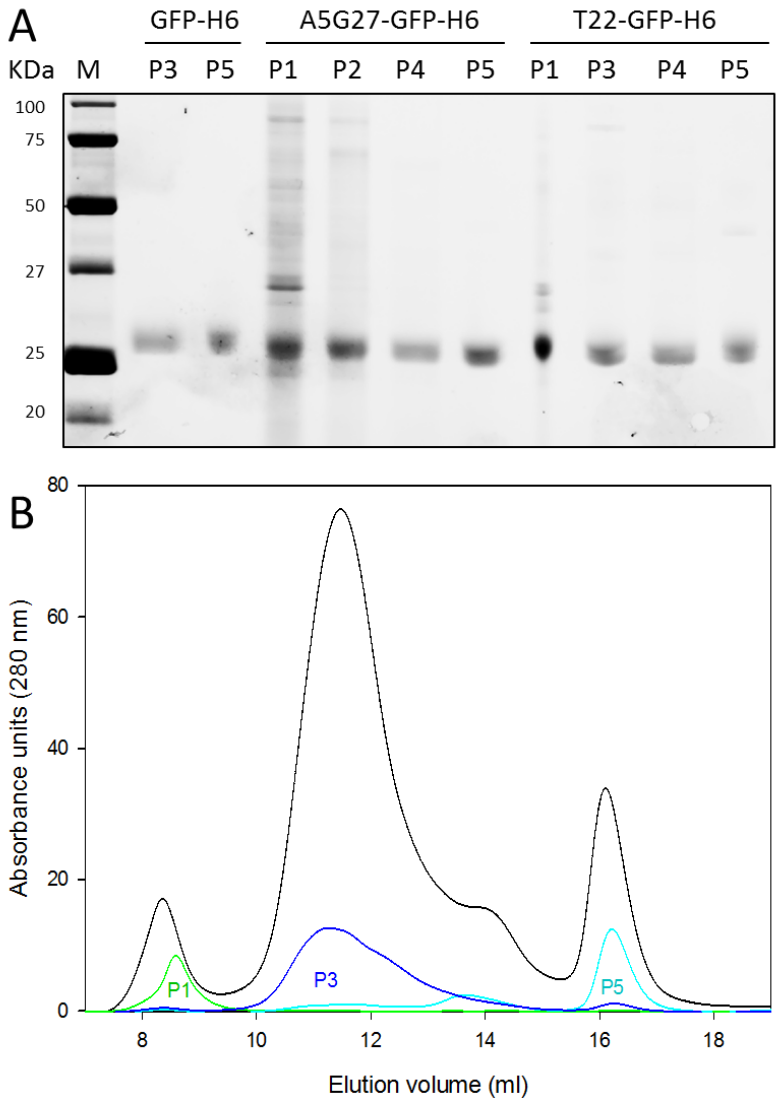

Supplementary Figure 3. Stability of protein conformations. A) Integrity of each protein population visualized on TGX stain-free SDS-PAGE gels. T22-GFP-H6 was produced in KPM335 (IMAC fraction 1). B) Structural stability of main T22-GFP-H6 protein oligomers produced in KPM335 (IMAC fraction 1), represented by coincident populations upon SEC separation (colour lines) and in the initial SEC analysis of the IMAC purified protein (black line). Similar matching curves have been obtained when analysing the main populations of the rest of proteins (not shown).

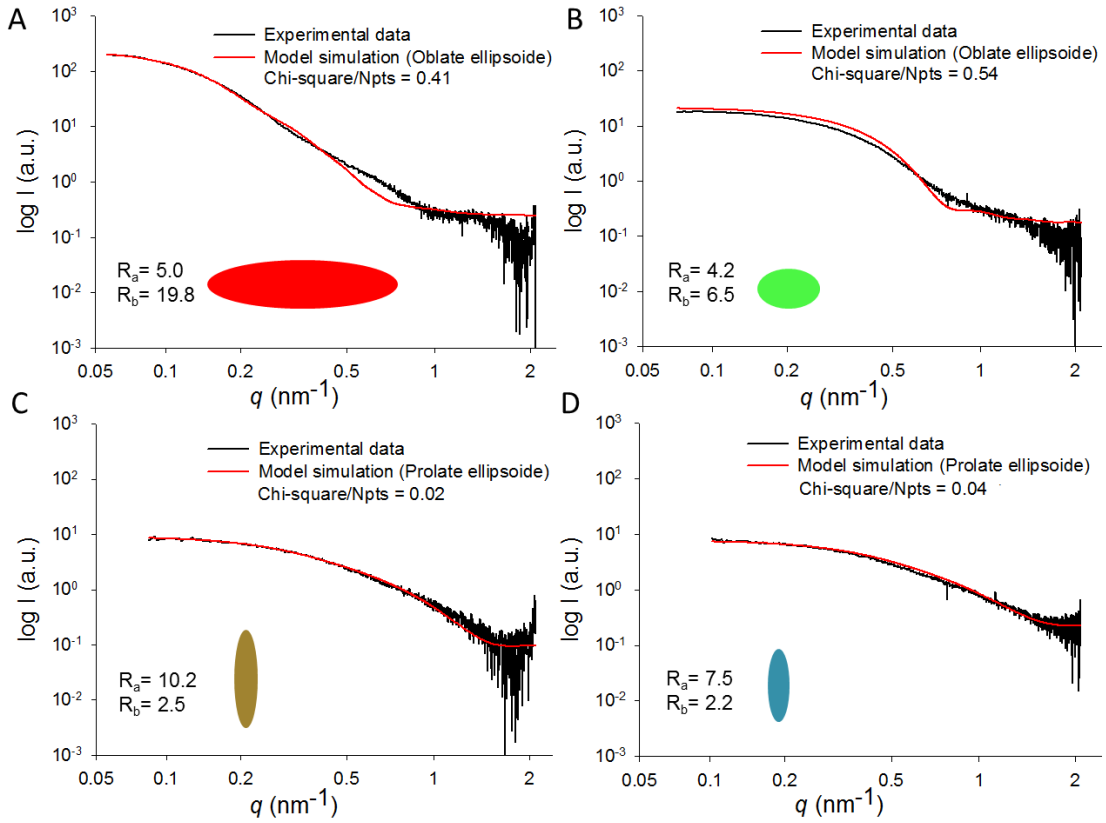

Supplementary Figure 4. Morphometric characterisation of T22-GFP-H6 KPM335 IMAC fraction 2 oligomers. SAXS data P1 (A), P2 (B), P4 (C) and P5 (D) (black dots) were fitted to ellipsoidal form factor simulations (red line). The Chi-square values for the different fittings are displayed on the graphs. Radius A and radius B (vertical and horizontal radius respectively) calculated with SasView and the shaped figure are also shown. Shapes within the panels correspond to the particle form and their colours to the peak in the plots from Figure 1 A.

Supplementary Table 1. Quantitative analysis of separated protein oligomers. Width and length of each oligomeric population determined from TEM images using DigitalMicrograph software. Values are expressed as mean ± standard error of mean. Peak numbers and colours are as in Figure 1 B.

Protein	Population	Width (nm)	Length (nm)
GFP-H6 BL21 (DE3)	P5	--	--
A5G27-GFP-H6 BL21 (DE3)	P1	15.2 ± 1.9	18.6 ± 1.1
	P2	12.1 ± 0.2	13.8 ± 0.2
	P5	5.4 ± 0.1	7.0 ± 0.1
T22-GFP-H6 Origami B	P1	15.9 ± 0.3	19.5 ± 0.6
	P2	10.1 ± 0.4	11.4 ± 0.5
	P5	5.1 ± 0.2	6.9 ± 0.4
T22-GFP-H6 KPM335 IMAC fraction 1	P1	12.7 ± 0.5	19.5 ± 0.6
	P3	9.1 ± 0.2	9.2 ± 0.2
	P4	5.9 ± 0.3	8.4 ± 0.6
	P5	4.1 ± 0.2	6.1 ± 0.4
T22-GFP-H6 KPM335 IMAC fraction 2	P1	15.6 ± 0.6	19.8 ± 0.5
	P2	11.5 ± 0.5	12.6 ± 0.6
	P4	4.1 ± 0.2	7.7 ± 0.1
	P5	4.5 ± 0.1	5.7 ± 0.2